Phase-space dependence of particle-ratio fluctuations in Pb+Pb collisions from 20A to 158A GeV beam energy

T. Anticic[21], B. Baatar[8], D. Barna[4], J. Bartke[6], H. Beck[9], L. Betev[10], H. Białkowska[18], C. Blume[9], B. Boimska[18], J. Book[9], M. Botje[1], P. Bunčić[10], P. Christakoglou[1], P. Chung[17], O. Chvala[14], J. Cramer[15], V. Eckardt[13], Z. Fodor[4], P. Foka[7], V. Friese[7], M. Gaździcki[9,11], K. Grebieszkow[20], C. Höhne[7], K. Kadija[21], A. Karev[10], V. Kolesnikov[8], M. Kowalski[6], D. Kresan[7], A. Laszlo[4], R. Lacey[17], M. van Leeuwen[1], M. Maćkowiak-Pawłowska[9,20], M. Makariev[16], A. Malakhov[8], G. Melkumov[8], M. Mitrovski[9], S. Mrówczyński[11], G. Pálla[4], A. Panagiotou[2], W. Peryt[20], J. Pluta[20], D. Prindle[15], F. Pühlhofer[12], R. Renfordt[9], C. Roland[5], G. Roland[5], M. Rybczyński[11], A. Rybicki[6], A. Sandoval[7], A. Rustamov[9], N. Schmitz[13], T. Schuster[9], P. Seyboth[13], F. Siklér[4], E. Skrzypczak[19], M. Słodkowski[20], G. Stefanek[11], R. Stock[9], H. Ströbele[9], T. Susa[21], M. Szuba[20], D. Varga[3], M. Vassiliou[2], G. Veres[4], G. Vesztergombi[4], D. Vranić[7], Z. Włodarczyk[11], A. Wojtaszek-Szwarc[11]

[1] *NIKHEF, Amsterdam, Netherlands.*

[2] *Department of Physics, University of Athens, Athens, Greece.*

[3] *Eötvös Loránt University, Budapest, Hungary.*

[4] *Wigner Research Center for Physics, Hungarian Academy of Sciences, Budapest, Hungary.*

[5] *MIT, Cambridge, Massachusetts, USA.*

[6] *H. Niewodniczański Institute of Nuclear Physics, Polish Academy of Sciences, Cracow, Poland.*

[7] *GSI Helmholtzzentrum für Schwerionenforschung GmbH, Darmstadt, Germany.*

[8] *Joint Institute for Nuclear Research, Dubna, Russia.*

[9] *Fachbereich Physik der Universität, Frankfurt, Germany.*

[10] *CERN, Geneva, Switzerland.*

[11] *Institute of Physics, Jan Kochanowski University, Kielce, Poland.*

[12] *Fachbereich Physik der Universität, Marburg, Germany.*

[13] *Max-Planck-Institut für Physik, Munich, Germany.*

[14] *Institute of Particle and Nuclear Physics, Charles University, Prague, Czech Republic.*

[15] *Nuclear Physics Laboratory, University of Washington, Seattle, Washington, USA.*

[16] *Institute for Nuclear Research and Nuclear Energy, BAS, Sofia, Bulgaria.*

[17] *Department of Chemistry, Stony Brook University (SUNYSB), Stony Brook, New York, USA.*

[18] *National Center for Nuclear Research, Warsaw, Poland.*
[19] *Institute for Experimental Physics, University of Warsaw, Warsaw, Poland.*
[20] *Faculty of Physics, Warsaw University of Technology, Warsaw, Poland.*
[21] *Rudjer Boskovic Institute, Zagreb, Croatia.*
*

(Dated: July 1, 2013)

Abstract

A novel approach, the identity method, was used for particle identification and the stdudy of fluctuations of particle yield ratios in Pb+Pb collisions at the CERN SPS. This procedure allows to unfold the moments of the unknown multiplicity distributions of protons (p), kaons (K), pions (π) and electrons. Using these moments the excitation function of the fluctuation measure ν_{dyn}[A,B] was measured, with A and B denoting different particle types. The obtained energy dependence of ν_{dyn} agrees with previously published NA49 results on the related measure σ_{dyn}. Moreover, ν_{dyn} was found to depend on the phase space coverage for $[K, p]$ and $[K, \pi]$ pairs. This feature most likely explains the reported differences between measurements of NA49 and those of STAR in central Au+Au collisions.

*Corresponding author: a.rustamov@cern.ch

I. INTRODUCTION

As the fundamental theory of strong interactions, Quantum Chromodynamics (QCD), is asymptotically free, the matter created at high temperature and/or high density is expected to be in a state of quasi-free quarks and gluons referred to as the Quark-Gluon Plasma (QGP). Lattice QCD calculations can study this non-perturbative regime of QCD [1] and allow a quantitative investigation of the QGP properties. A first order phase boundary is expected to separate high temperature hadron matter from the QGP for large net baryon density and is believed to end in a critical point [2]. By colliding heavy-ions at high energies one hopes to heat and/or compress the matter to energy densities at which the production of the QGP begins. A wealth of ideas has been proposed to explore the properties and the phase structure of strongly interacting matter. Event-by-event fluctuations of various observables may be sensitive to the transitions between hadronic and partonic phases [3, 4]. Moreover, the location of the critical point may be signalled by a characteristic pattern in the energy and system size dependence of the measured fluctuation signals.

Pb+Pb reactions were investigated at the CERN SPS since 1994 by a variety of experiments at the top SPS energy. Many of the predicted signals of the QGP were observed [5] but their uniqueness was in doubt. Motivated by predictions of the SMES model [6] of characteristic changes of hadron production properties at the onset of QGP creation (onset of the deconfinement) the NA49 experiment performed a scan of the entire SPS energy range, from 158A down to 20A GeV. The predicted features were found at an energy of about 30A GeV in central Pb+Pb collisions [7] thereby indicating the onset of deconfinement in collisions of heavy nuclei in the SPS energy range. These observations have recently been confirmed by the RHIC beam energy scan and the expected trend towards higher energy is consistent with LHC data [8].

Motivated by these findings the NA49 Collaboration has started to explore the phase diagram of strongly interacting matter, with the aim of searching for indications of the first oder transition and the critical point by studying several measures of fluctuations. In particular, the energy dependence of dynamical event-by-event fluctuations of the particle composition was investigated using the measure $\sigma_{dyn}(A/B)$ with A and B denoting the multiplicities of differnt particle species. An increasing trend of σ_{dyn} for both K/p and K/π ratios towards lower collision energies was observed [9–11]. In contrast, recent results of the

STAR experiment from the Beam Energy Scan (BES) at RHIC show practically no energy dependence of the related event-by-event fluctuation measure ν_{dyn} [13] for [K, p] and [K, π] pairs [12]. The comparison between NA49 and corresponding STAR results were performed using the relation

$$\nu_{dyn} = sgn(\sigma_{dyn})\sigma^2_{dyn}. \quad (1)$$

However, the accuracy of this relation decreases inversely with multiplicity, i.e. at lower energies this relation is only approximate. In order not to rely on this approximation the fluctuation measure ν_{dyn} was directly reconstructed in this paper using a novel identification scheme, the identity method [14, 15]. The procedure avoids event-by-event particle ratio fits and the use of mixed events necessary to subtract the artificial correlations introduced by the fits. Moreover, the much improved statistical power allows to study the effects of the different phase space coverage of the NA49 (forward rapidities) and STAR (central rapidity, without low p_T range) experiments.

The paper is organized as follows. Details about the detector setup and the data are given in section II. Section III discusses the event and track selection criteria. The novel features of this analysis, i.e. the particle identification procedure and the extraction of the moments of the multiplicity distributions are discussed in sections IV and V respectively. Section VI presents the estimates of statistical and systematic uncertainties. Results on ν_{dyn} and their phase-space dependence are discussed in sections VII and VIII. Finally, section IX summarizes the paper.

II. EXPERIMENTAL SETUP AND THE DATA

This paper presents results for central Pb+Pb collisions at projectile energies of $20A$, $30A$, $40A$, $80A$ and $158A$ GeV recorded by the NA49 experiment (for a detailed description of the NA49 apparatus cf. Ref. [16]). The principal tracking detectors are four large volume Time Projection Chambers (TPC) with two of them, Vertex TPCs (VTPC1 and VTPC2), placed inside superconducting dipole magnets with a combined maximum bending power of 9 Tm for a length of $7m$. Care was taken to keep the detector acceptance approximately constant with respect to midrapidity by setting the magnetic field strength proportional to the beam energy. Particle identification in this analysis is achieved by simultaneous measurement of

Beam energy [GeV]	$\sqrt{s_{NN}}$	N_{events}	$< N^{all} >$	$< N^{pos.} >$
20A	6.3	169k	63	46
30A	7.6	179k	113	75
40A	8.7	195k	159	99
80A	12.3	136k	315	181
158A	17.3	125k	560	310

Table I. The statistics corresponding to the 3.5% most central central Pb+Pb collisions used in this analysis.

particle momenta and their specific energy loss dE/dx in the gas volume of the main TPCs (MTPC-L and MTPC-R). These are located downstream of the magnets on either side of the beam, have large dimensions (4 $m \times 4m \times 1.2m$) and feature 90 readout pad rows, providing an energy loss measurement with a resolution of about 4%. In the experiment Pb beams with intensity of 10^4 ions/s were incident on a thin lead foil located 80 cm upstream of the VTPC-1. For 20A - 80A GeV and 158A GeV the target thicknesses amount to 0.224 g/cm^2 and 0.336 g/cm^2 respectively. The centrality of a collision was determined based on the energy of projectile spectators measured in the veto (VCAL) calorimeter which is located 26 m behind the target and covers the projectile-spectator phase space region. A collimator in front of the calorimeter was adjusted for each energy in such a way that all projectile spectator protons, neutrons and beam fragments could reach the veto calorimeter while keeping the number of produced particles hitting the calorimeter as small as possible.

III. EVENT AND TRACK SELECTION CRITERIA

The only event selection criterion used in this analysis is a centrality cut based on the energy (E_{Cal}) of forward going projectile spectators measured in VCAL. The data were recorded with an online VCAL cut accepting the 7% and 10% most central Pb+Pb collisions for 20A - 80A GeV and 158A GeV respectively. Using an offline cut on E_{Cal} event samples of the 3.5% most central reactions were selected which in the Glauber Monte Carlo Model

corresponds to about 367 wounded nucleons and an impact parameter range of b $<$ 2.8 fm. To ensure better particle separation only the tracks with large track length (better energy loss resolution) in the MTPCs were used for further analysis. For this purpose we distinguish between the number of potential and the number of reconstructed dE/dx points. The former was estimated according to the position of the track in space together with the known TPC geometry, while the latter represents the number of points reconstructed by the cluster finder algorithm. The following track selection criteria referred to as the "loose cuts" are used for the main analysis:

- Number of reconstructed points in the MTPCs: > 30.
- The ratio of the number of reconstructed points in all TPCs (VTPCs + MTPCs) to the number of potential points in all TPCs: > 0.5.

These selections reduce the acceptance of the particles to the forward rapidity regions in the center-of-mass reference frame. In order to study the systematic uncertainties of the final results due to the applied track cuts another set of cuts ("tight cuts") was employed in addition to the "loose cuts":

- The number of potential points in at least one of VTPC1 or VTPC2 > 10 and in the MTPCs > 30.
- The ratio of the number of reconstructed points to the number of potential points in the selected TPC(s): > 0.5.
- The track should be fitted to the primary vertex.
- The distance between the closest point on the extrapolated track to the main vertex position should be less than $4cm$ in x (bending plane) and less than $2cm$ in y (vertical).

IV. PARTICLE IDENTIFICATION

Particle identification (PID) in this analysis is achieved by correlating the measured particle momentum with its specific energy loss dE/dx in the gas volume of the MTPCs. The key problem of particle identification by dE/dx measurement is the fluctuation of ionization

losses. The energy loss distribution has a long tail for large values. Its shape was first calculated in Ref. [17] and is referred to as the Landau distribution. To improve the resolution of the dE/dx measurement, multiple samplings in pad rows along the track are performed. An appropriate estimate of dE/dx is then calculated as a truncated mean of the distribution of charge measurements. To obtain the contributions of different particle species fits of the inclusive dE/dx distributions (see Ref. [18] for details) were performed separately for negatively and positively charged particles in bins of total laboratory momentum p, transverse momentum ($\mathrm{p}_\perp$) and azimuthal angle (ϕ). Bins with less than 3000 entries were not used in the analysis to ensure sufficient statistics in each bin for the fitting algorithm. The distribution of the number of measured dE/dx points in a selected bin is demonstrated in Fig. 1. As for each track the energy loss is measured multiple times the inclusive dE/dx distribution (averaged over all events for the particular bin) for each particle type i is represented by a weighted sum of Gaussian functions:

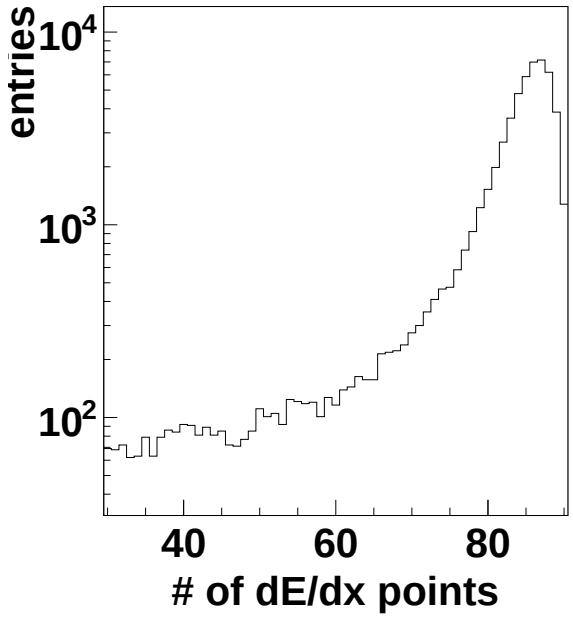

Figure 1. (Color Online)Distribution of number of measured dE/dx points along the tracks for the phase space bin p, $\mathrm{p}_\perp$, ϕ **give ranges and beam energy !**.

$$F_i\left(\frac{dE}{dx}\equiv x\right)=\frac{1}{C}\sum_n\frac{N_n}{\sqrt{2\pi}\sigma_{i,n}}\exp\left[-\frac{1}{2}\left(\frac{x-\bar{x_i}}{(1\pm\delta)\sigma_{i,n}}\right)^2\right]. \quad (2)$$

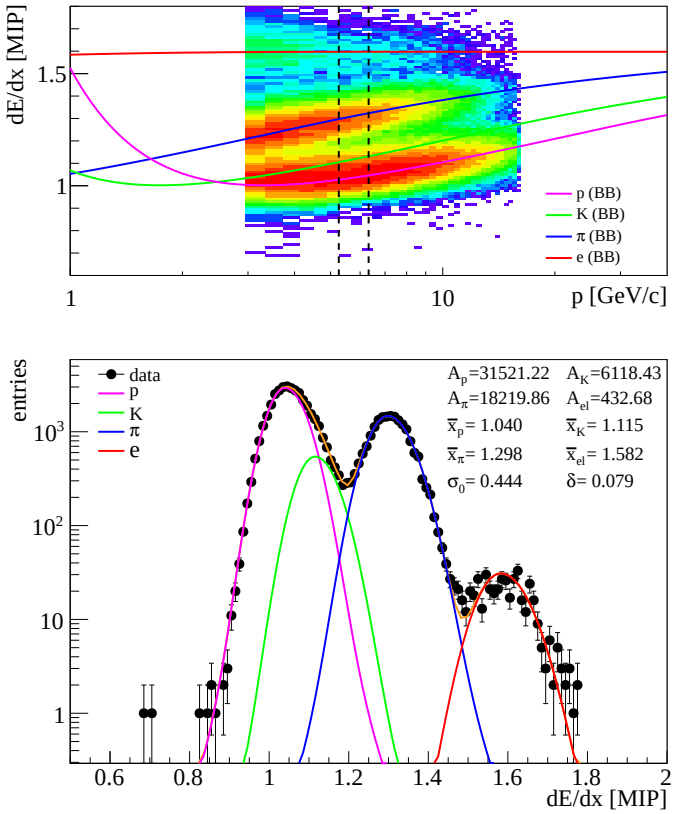

Figure 2. (Color Online)Upper panel: Measured dE/dx values as function of reconstructed momenta. Different lines correspond to calculations with Bethe-Bloch formula. Lower panel: A projection of the upper plot to Y axis in a selected momentum interval indicated by vertical dashed lines. Colored lines represent the dE/dx distribution functions of different particles using the formula 2 and fit parameters listed in the figure.

Here, N is the number of tracks with n dE/dx measurements, while $\sigma_{i,n}$ is the width of the Gaussian distribution which depends on particle type and the number of dE/dx measurements, n. δ is the asymmetry parameter which was introduced to account for the tails of the Landau distributions, which are still present even after truncation. The normalization constant C in Eq.(2) is $\sum_n N_n$, while $\sigma_{i,n}$ is parametrized as:

$$\sigma_{i,n} = \sigma_0 \left(\frac{\bar{x}_i}{\bar{x}_\pi} \right)^{\alpha} \frac{1}{\sqrt{N_n}}. \tag{3}$$

where α was estimated from the data and set to 0.625 [18].

The parameterisation of the total energy loss distribution is obtained by summing the

functions F_i over the particle types.

$$F(x) = \sum_{i=p,K,\pi,e} A_i F_i(x). \tag{4}$$

with A_i being the yield of particle i in a given bin. As a result of the fitting this function to the experimental dE/dx distributions one obtains in each phase space bin the yield of particle i, A_i, the ratio of mean ionization loss $\bar{x}_i/\bar{x}_\pi$, the parameter σ_0 and the asymmetry parameter δ. The total number of fitted parameters is $2(i+1)$ with i denoting the number of particles. Obtained fit parameters, which are later used to access the dE/dx distribution functions (DF) of different particles, were stored in a lookup table. In the case of positive particles DFs of kaons are masked by the protons and the mean values for protons and kaons cannot be fitted uniquely. To circumvent this problem the fitting procedure was performed in two steps:

1. Start the fitting procedure with negatively charged particles. As for the studied energy range the number of antiprotons are small the pion and kaon peaks are essentially separated. Furthermore, to enhance the statistics integration is performed over the transverse momentum bins at this stage.

2. The fitting procedure was performed separately for negatively and positively particles in bins of p, $p_\perp$ and ϕ with the ratio $\frac{\bar{x_K}}{\bar{x_\pi}}$ fixed from step 1.

As an example, we present in the upper panel of Fig. 2 a scatter plot of measured dE/dx values versus the reconstructed momenta. The lower panel of Fig. 2 shows the projection of the upper plot onto the dE/dx axis in the selected momentum interval indicated by dashed vertical lines. The distribution functions of different particles obtained from formula Eq.(2) using the fit parameters listed in the figure are displayed by colored lines.

In figure 3 the ratios of mean energy losses between different particles are compared to corresponding ratios from the Bethe-Bloch parameterization. Figure 4 demonstrates the separation between fitted mean energy loss values of kaons and protons quantified as $|x_p - x_K|/x_p$ with x_p and x_K denoting the mean energy loss values for protons and kaons respectively.

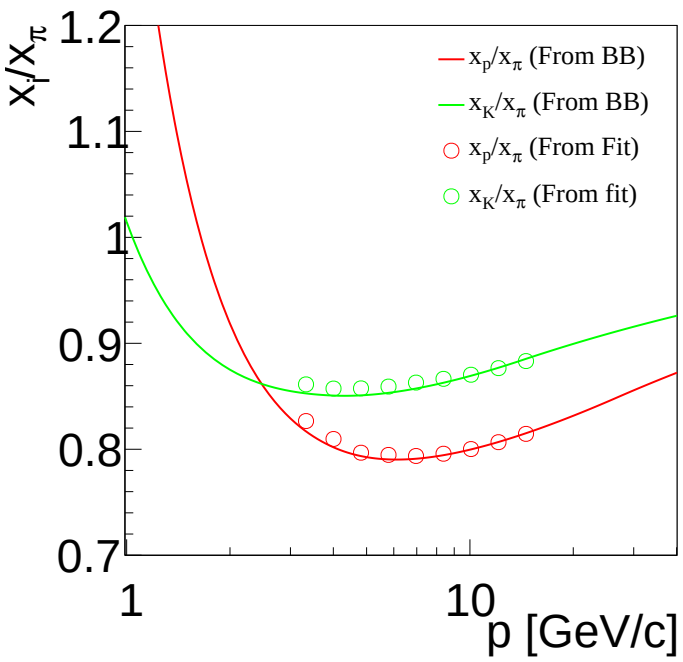

Figure 3. (Color Online) Ratio of fitted mean energy losses denoted by open symbols compared to corresponding ratios from the Bethe-Bloch parametrization. The deviation between fitted values and the Bethe-Bloch curve is below 1 %.

V. ANALYSIS METHOD

Most measures proposed for event-by-event fluctuations are defined as functions of moments of the unknown multiplicity distributions. In particular, the fluctuation measure ν_{dyn} depends on the first and all second (pure and mixed) moments of the multiplicity distributions of the studied particles species. The standard approach of finding the moments is to count the number of particles event-by-event. However, this approach is hampered by incomplete particle identification (overlapping dE/dx distribution functions), which can be taken care of by either selecting suitable phase space regions (where the distribution functions do not overlap) or by applying a fitting procedure event-by-event. The latter typically introduces artificial correlations which are usually corrected for by the event mixing technique. Here a novel approach, called *Identity Method* [14, 15, 19] is applied for the first time. The method follows a probabilistic approach which avoids the event-by-event fitting and allows to determine the moments of the multiplicity distribution by an unfolding procedure which

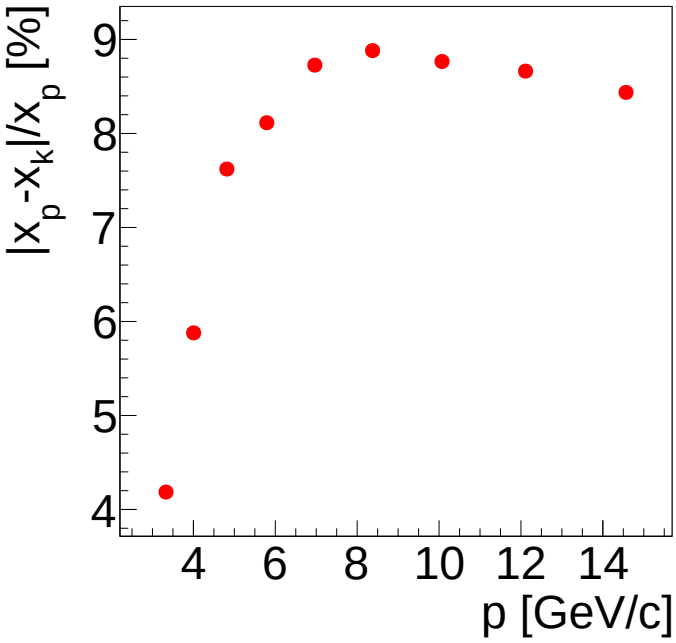

Figure 4. (Color Online) The difference between mean energy loss of kaons and protons normalized to the mean energy loss of protons.

has a rigorous mathematical derivation [15]. Thus there is no need for corrections based on event mixing. The method employs the fitted inclusive dE/dx distribution functions of particles, $\rho_j(x)$, with j standing for proton, kaon, pion and electron. Each event has a set of measured dE/dx values, x_i, corresponding to each track in the event. For each track in an event a probability w_j was estimated of being a particle j:

$$w_j(x_i) \equiv \frac{\rho_j(x_i)}{\rho(x_i)}, \tag{5}$$

where the values of $\rho_j(x_i)$ are calculated using the parameters stored in the lookup table of fitted DFs in the appropriate phase space bin and: **we should show the explicit relation between the DFs and ρ_j !**

$$\rho(x_i) \equiv \sum_{j=p,K,\pi,e} \rho_j(x_i) \tag{6}$$

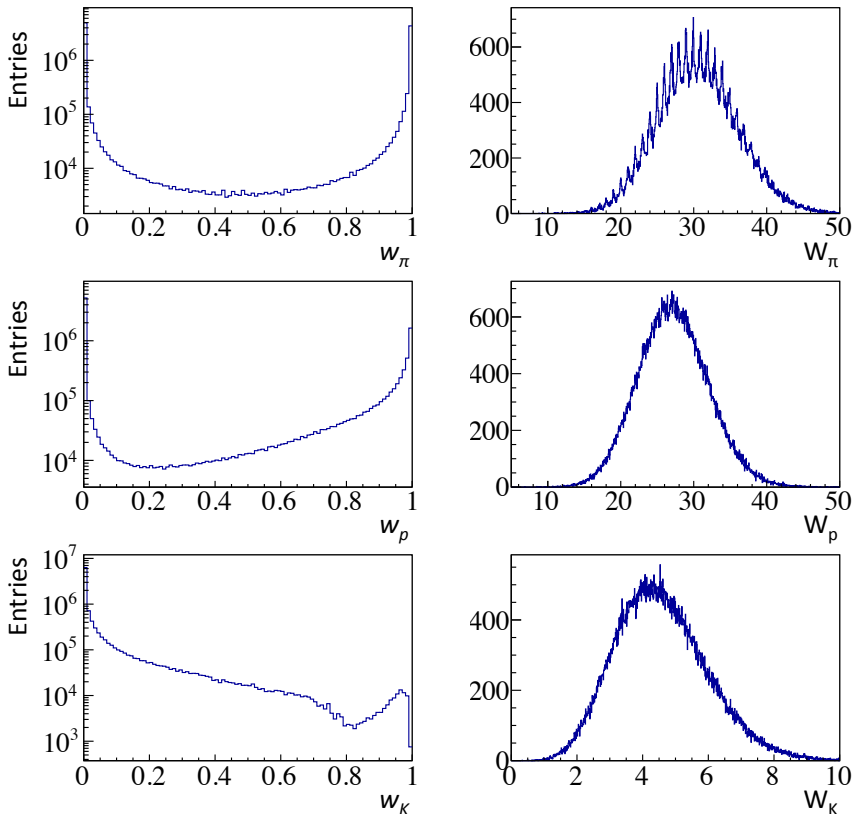

Figure 5. (Color Online) Distributions of w and W for different particle types.

Further an event variable (an approximation of the multiplicity of particle j in the event) W_j is defined as:

$$W_j = \sum_{i=1}^{n} w_j(x_i) \tag{7}$$

where n is the total number of selected tracks in the given event. Examples of distributions of w and W for π, K and p are shown in Fig.5.

As the introduced W quantities are calculated for each event, one obtains all second moments of the W quantities by straightforward averaging over the events. Finally, using the Identity Method one unfolds the second moments of the true multiplicity distributions from the moments of the W quantities [15]. Obtained results (second moments) for the 3.5% most central Pb+Pb collisions at different projectile energy are listed in the lower part of Table II. The mean multiplicities (first moments) shown in the upper part of Table II are the results of integration of the respective DFs. The Identity Method has been tested in numerous simulations reported in Ref. [19]. A direct experimental verification of the

	20A GeV	30A GeV	40A GeV	80A GeV	160A GeV
$\langle N_p \rangle$	27.0973	34.7303	37.9555	47.0417	68.7236
$\langle N_\pi \rangle$	30.5294	66.444	103.0170	226.7240	414.633
$\langle N_K \rangle$	4.6706	9.4111	13.8889	31.5464	57.7823
$\langle N_p^2 \rangle$	759.938	1238.09	1475.89	2254.3501	4780.52
$\langle N_\pi^2 \rangle$	963.6	4485.3599	10731.4004	51764.3984	172811.0
$\langle N_K^2 \rangle$	26.3952	98.0613	207.272	1030.0601	3415.6899
Cov$[N_p, N_\pi]$	2.12073	4.33984	9.04827	22.61761	44.02652
Cov$[N_p, N_K]$	-0.74811	-0.68567	0.39282	2.41379	10.92219
Cov$[N_K, N_\pi]$	-1.0250	-1.3868	0.28719	15.84394	81.75147

Table II. Upper part: mean multiplicities of $p + \bar{p}$, $\pi^+ + \pi^-$, and $K^+ + K^-$ for the 3.5% most central Pb+Pb collisions calculated by summing the integrals of respective DFs over phase-space bins. Lower part: reconstructed second moments of the multiplicity distributions of $p+\bar{p}$, $\pi^+ + \pi^-$, and $K^+ + K^-$ for the 3.5% most central Pb+Pb collisions. The mixed moments are presented in terms of covariances, Cov$[N_1, N_2] =< N_1 N_2 > - < N_1 >< N_2 >$. For 20$A$ and 30A GeV values for Cov$[N_p, N_K]$ and Cov$[N_p, N_K]$ are negative.

method can be provided by investigating the energy dependence of the scaled variance ω of the negatively charged pion multiplicity distribution.

$$\omega = \frac{Var(N)}{< N >} = \frac{< N^2 > - < N >^2}{< N >} \tag{8}$$

For this purpose two independent analyses were performed: (i) using the reconstructed moments for negatively charged pions (from the Identity Method) and (ii) counting the negatively charged particles event-by-event (i.e without employing the Identity Method). The results of these analyses are presented in Fig. 6 by blue squares for case (i) and by red triangles for case (ii). As the majority of negative particles are pions the remarkable agreement between the results of these two independent approaches is a direct experimental verification of the Identity Method.

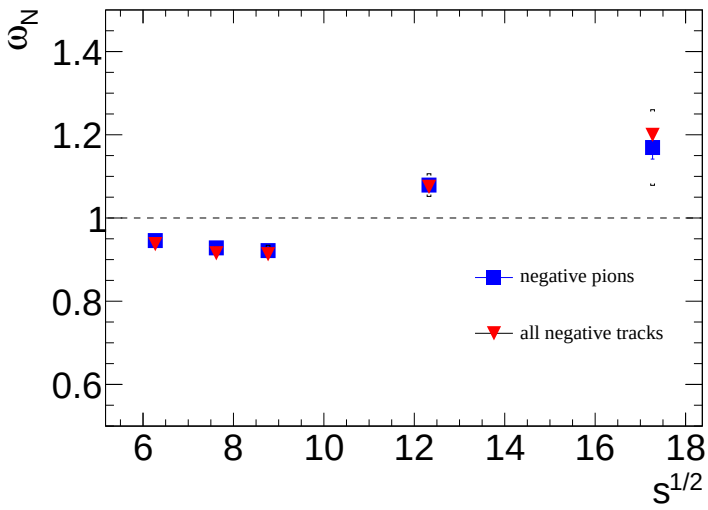

Figure 6. (Color Online) The energy dependence of the scaled variance ω of the negatively charged pion multiplicity distribution is plotted as blue squares. The red squares are estimates based on direct event-by-event counting of all negative particles. The remarkable agreement between these results is an experimental verification of the Identity Method.

VI. STATISTICAL AND SYSTEMATIC ERROR ESTIMATES

The statistical errors of the reconstructed moments of the multiplicity distributions result from the errors on the parameters of the fitted distributions $\rho_j(x)$ and from the errors of the W_j quantities. Typically these two sources of errors are correlated. Fluctuation observables are usually built up from several moments of the multiplicity distributions. The standard error propagation is complicated and inconvenient. Therefore the subsmaple approach was chosen to evaluate the statistical uncertainties. One first randomly subdivides the data into n subsamples and for each subsample then reconstructs the moments M_n listed in Table II. In the second step the statistical error of each moment M is calculated as:

$$\sigma_{<M>} = \frac{\sigma}{\sqrt{n}}, \tag{9}$$

where

$$< M >= \frac{1}{n} \sum M_n, \tag{10}$$

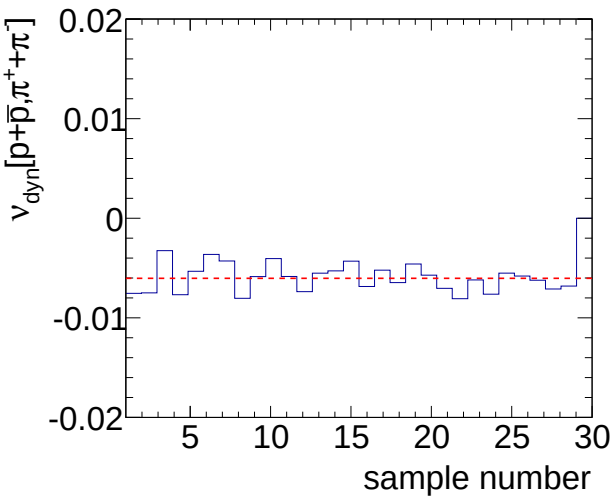

Figure 7. (Color Online) Reconstructed values $\nu_{dyn}[p+\bar{p}, \pi^+ + \pi^-]$ as function of subsample number. The dashed red line indicates the averaged value of ν_{dyn} over samples.

and

$$\sigma = \sqrt{\frac{\sum (M_i - < M >)^2}{n-1}}. \tag{11}$$

The same procedure is followed for the fluctuation quantities, e.g. ν_{dyn}, which are functions of the moments. An example is shown in Fig. 7.

Next, possible biases of the analysis procedure are studied using mixed events. Each event i was constructed by randomly selecting a reconstructed track (including the dE/dx measurement)from following j events, with j corresponding to the number of reconstructed tracks in the event i. The results for $\nu_{dyn}[K^+ + K^-, \pi^+ + \pi^-]$ for mixed events are presented in Fig. 8 by red open circles. As expected the reconstructed values of ν_{dyn} are vanishing independent of energy.

Furthermore, systematic uncertainties stemming from the quality of the fit functions were investigated with the help of mixed events. Even though the 2-step fitting procedure discussed in section IV was used to determine the DFs, it remains a challenge to properly fit the kaon positions. Nearly in all relevant phase-space intervals the measured energy loss distributions of kaons are overlapping with those of pions and protons. To study the influence of possible systematic shifts in fit parameters on the extracted moments the fitted positions of kaons were shifted artificially by 1 % in both directions. The dashed-green lines in Fig 9 show the artificially shifted dE/dx distribution functions of kaons. Results

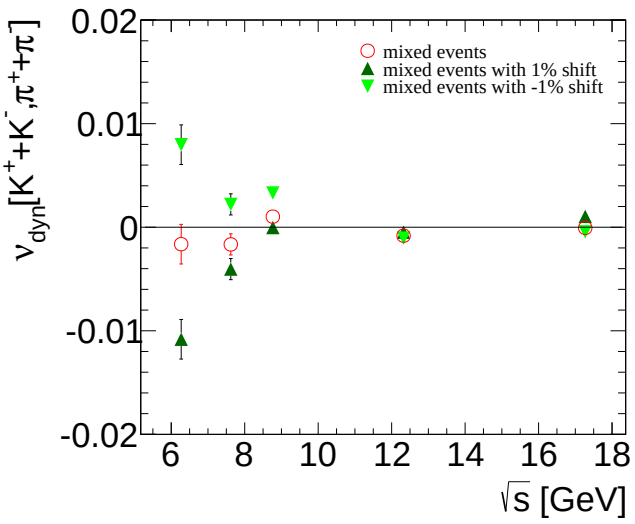

Figure 8. (Color Online) $\nu_{dyn}[K^+ + K^-, \pi^+ + \pi^-]$ for mixed events is shown versus energy by red open circles. Dark-green (light-green) triangles represent the results obtained with the artificially shifted kaon positions by 1% (-1%).

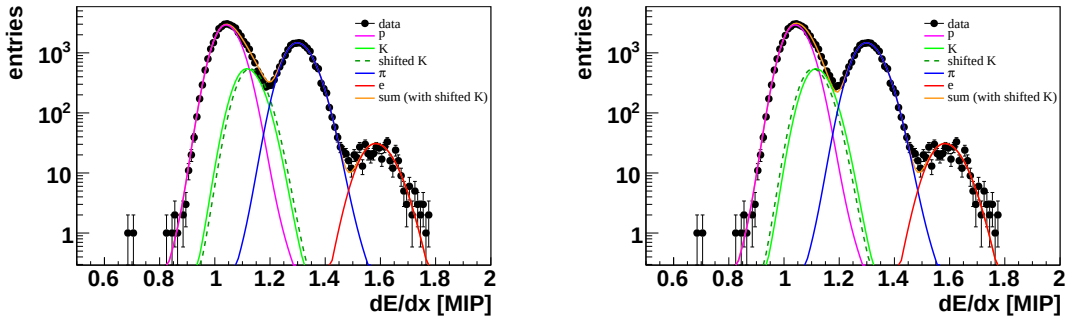

Figure 9. (Color Online) Energy loss distributions in the selected phase space bin corresponding to Fig. 2 with superimposed fit functions for protons, pions, kaons and electrons shown by colored solid lines. The dashed green lines correspond to artificially shifted positions of kaons by 1% (left) and -1% (right). The shifted distribution functions were used to investigate the systematic errors stemming from the particle identification (dE/dx fitting) procedure.

for $\nu_{dyn}[K^+ + K^-, \pi^+ + \pi^-]$ obtained with these shifted kaon distribution functions for the mixed events are plotted as green triangles in Fig. 8. At lower beam energies one observes a strong dependence of the results on kaon positions.

VII. RESULTS ON THE FLUCTUATION MEASURE ν_{dyn}

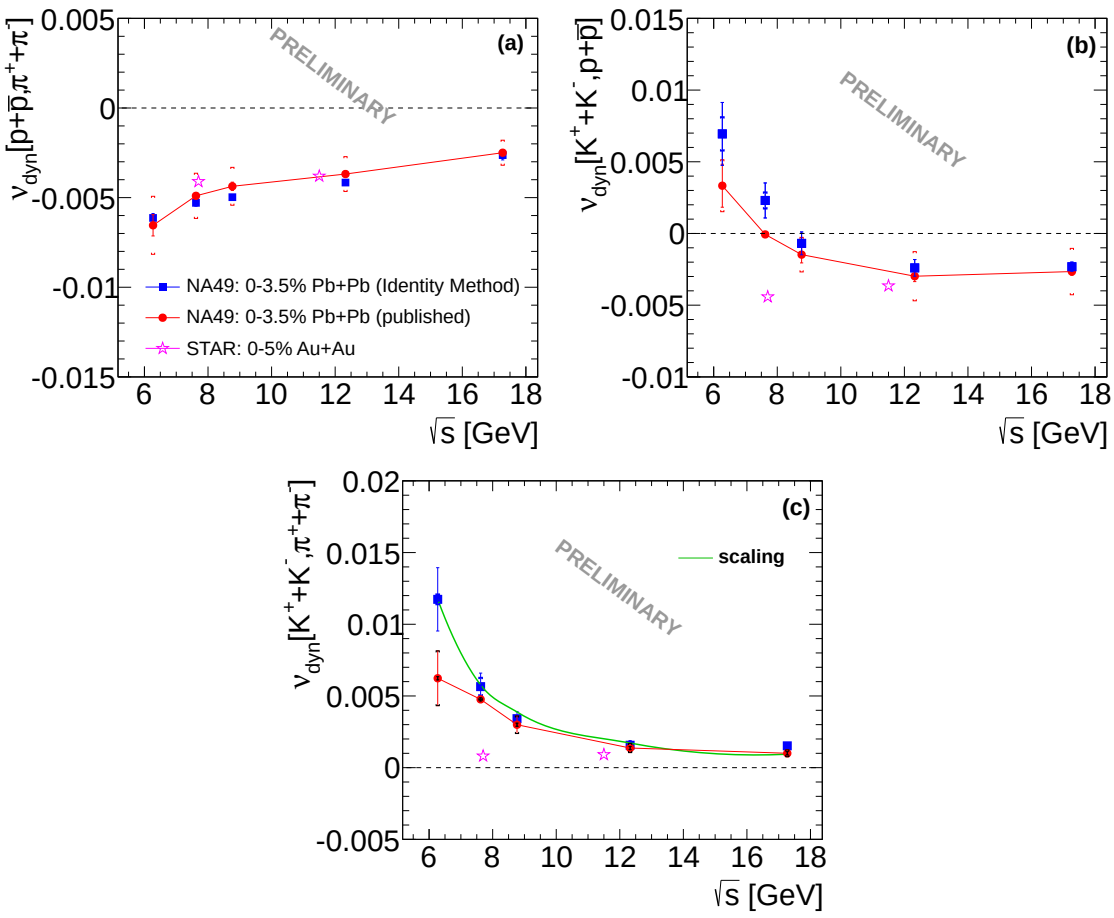

Figure 10. (Color Online) Energy dependence of (a) $\nu_{dyn}[p+\bar{p},\pi^+ +\pi^-]$, (b) $\nu_{dyn}[K^+ +K^-,p+\bar{p}]$ and (c) $\nu_{dyn}[K^+ +K^-,\pi^+ +\pi^-]$. Results from the Identity Method for central Pb+Pb data of NA49 are shown by blue squares. Published NA49 results, converted from σ_{dyn} to ν_{dyn} are indicated by circles (the lines join the measurements for clarity). Stars represent results of the STAR collaboration for central Au+Au collisions. In addition, for the case (c), the energy dependence predicted by Eq.(14) is displayed by the blue curve, which is consistent with the experimentally established trend.

The measure $\nu_{dyn}[A,B]$ of dynamical event-by-event fluctuations of the particle composition is defined as [13]:

$$\nu_{dyn}[A,B] = \frac{\langle A(A-1)\rangle}{\langle A\rangle^2} + \frac{\langle B(B-1)\rangle}{\langle B\rangle^2} - 2\frac{\langle AB\rangle}{\langle A\rangle\langle B\rangle}, \tag{12}$$

where A and B stand for multiplicities of different particle species. As seen from the definition Eq.(12) the value of ν_{dyn} vanishes when the multiplicity distributions of particles

A and B follow the Poisson distribution and when there are no correlations between these particles ($< AB >=< A >< B >$). On the other hand a positive correlation term reduces the value of ν_{dyn}, while an anticorrelation increases it. Inserting the values of the reconstructed moments from Table II into Eq.(12) one obtains the values of $\nu_{dyn}[p+\bar{p}, \pi^+ + \pi^-]$, $\nu_{dyn}[K^+ + K^-, p+\bar{p}]$ and $\nu_{dyn}[K^+ + K^-, \pi^+ + \pi^-]$. These results are represented by blue squares in Fig. 10. Statistical errors σ_{stat} were estimated using the subsample method discussed in section VI. Systematic uncertainties due to the applied track selection criteria were estimated by calculating ν_{dyn} separately for tracks selected by "loose" (ν_{dyn}^{loose}) and "tight" (ν_{dyn}^{tight}) cuts (see section III). Final results are then presented as:

$$\nu_{dyn}[A,B] = \frac{\left\langle \nu_{dyn}^{loose} \right\rangle + \left\langle \nu_{dyn}^{tight} \right\rangle}{2} \pm \sigma_{stat} \pm \frac{1}{2}\left| \left\langle \nu_{dyn}^{loose} \right\rangle - \left\langle \nu_{dyn}^{tight} \right\rangle \right| \tag{13}$$

These results are consistent with the previously published NA49 measurements of the related measure σ_{dyn} [9, 10] indicated by red circles in Fig. 10. We thus conclude that the increasing trend of the excitation functions of $\nu_{dyn}[K^+ + K^-, p+\bar{p}]$ and $\nu_{dyn}[K^+ + K^-, \pi^+ + \pi^-]$ at low energies are observed by two independent analyses of the NA49 data on central Pb+Pb collisons. Also presented in Fig. 10 are the STAR results (purple stars) from the RHIC Beam Energy Scan (BES) program [12] for central Au+Au collisions, which clearly differ at low energies. However, as mentioned above, the phase space coverage of NA49 and STAR are not the same. The consequences will be discussed below.

VIII. PHASE SPACE DEPENDENCE OF ν_{dyn} MEASUREMENTS

The investigation presented in this section attempts to shed light on the cause of the differences between the results from STAR and NA49 on fluctuations of identified hadrons. Two sources were studied: the dependence of ν_{dyn} on the multiplicity of the particles entering the analysis and a possible sensitivity of ν_{dyn} to the covered phase space region.

Indeed, it was found in Ref. [20] that ν_{dyn} exhibits an intrinsic dependence on the multiplicities of accepted particles. Since multiplicities increase with collision energy this leads to a trivial energy dependence of ν_{dyn}:

$$\nu_{dyn}(x) = \nu_{dyn}(\sqrt{s_{NN}}) \frac{\left[\frac{1}{<A>} + \frac{1}{<B>}\right]_x}{\left[\frac{1}{<A>} + \frac{1}{<B>}\right]_{\sqrt{s_{NN}}}}, \tag{14}$$

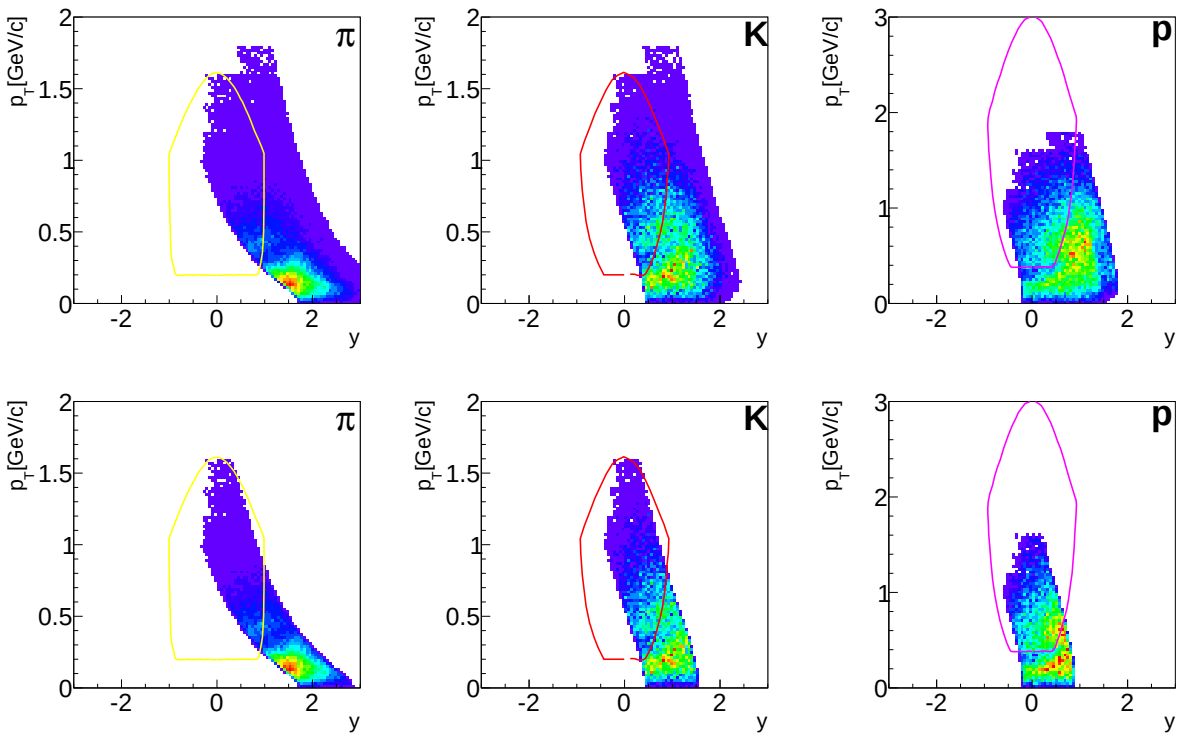

Figure 11. (Color Online) Phase space coverage for identified pions, kaons and protons in the acceptance of the NA49 experiment for the Pb+Pb collisions at 30A GeV/c (upper panels). Lower panels illustrate an example of a restriction of the phase-space coverage to better match the region covered by STAR (indicated by solid lines) at the corresponding beam energy.

where $\sqrt{s_{NN}}$ is a reference energy at which the value of measured ν_{dyn} can be chosen. The energy dependence predicted by Eq.(14), with reference energy of $\sqrt{s_{NN}}$ ≈6.3 GeV (corresponding to 20A GeV laboratory momentum), is illustrated for $\nu_{dyn}[K^+ + K^-, \pi^+ + \pi^-]$ in Fig. 10(c) by the green curve.

Here we should also dicuss the scaling for other particle combinations and what happens to the STAR results when one applies multiplicity scaling !

It was already mentioned in section I that published NA49 and STAR measurements were performed in significantly different phase space regions. As an example Fig. 11 illustrates the phase space coverage of pions, kaons and protons at 30A GeV projectile energy in the acceptance of the NA49 detector. In the same figure the acceptance of the STAR apparatus at corresponding center-of-mass energy is presented by colored lines. The dependence of ν_{dyn} on the selected phase space region was studied by performing the analysis in different phase

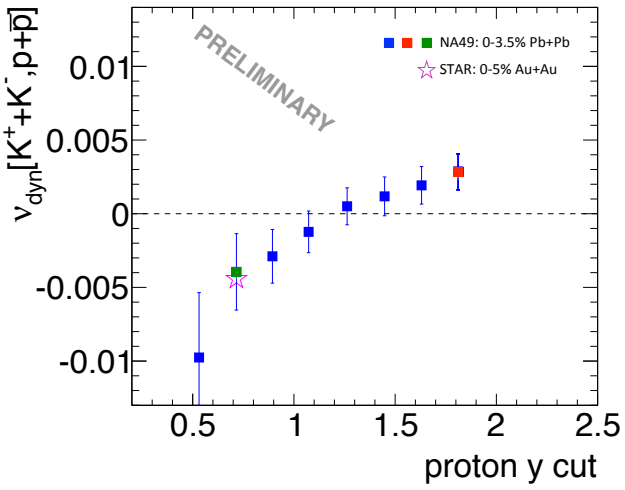

Figure 12. (Color Online) Phase space dependence of $\nu_{dyn}[K^+ + K^-, p + \bar{p}]$ for 30A GeV Pb+Pb collisions of NA49. Red and green squares correspond to the phase space bins illustrated in the upper and lower panels of Fig. 11 respectively. Blue squares are the NA49 results for other phase space bins. The result of the STAR experiment is plotted as the purple star at the corresponding NA49 phase space bin. The phase space region of the analysis is varied by an upper cut on the momentum (see text).

space bins stretching from a forward rapidity cut to mid-rapidity. Technically different phase space bins were selected by applying upper momentum cuts to the reconstructed tracks where the cut value corresponded to the momentum of a proton at p_T=0 with a chosen maximum rapidity. Thereafter this quantity will be called a proton rapidity cut. The upper panel of Fig. 11 illustrates one such phase space bin for 30A GeV Pb+Pb data. The reconstructed value of $\nu_{dyn}[K^+ + K^-, p + \bar{p}]$ in this bin is plotted as a red square in Fig. 12. Similarly the green square in Fig. 12 represents the reconstructed value of $\nu_{dyn}[K^+ + K^-, p + \bar{p}]$ corresponding to the phase space bin plotted in the lower panel of Fig. 11. Note that in this particular bin the NA49 point is consistent with the STAR result, which is shown by the purple star. This study demonstrates a strong phase space dependence of the resulting value of ν_{dyn} on the phase space coverage. Fig. 13 shows the dependence of ν_{dyn} for different combinations of particles at different energies. At 20A and 30A GeV $\nu_{dyn}[K^+ + K^-, p + \bar{p}]$ and $\nu_{dyn}[K^+ + K^-, \pi^+ + \pi^-]$ show a strong dependence on the extent of the phase space region and eventually hit the STAR point in a particular bin. Interestingly the acceptance dependence weakens above 30A GeV where no difference was observed with STAR. It is also

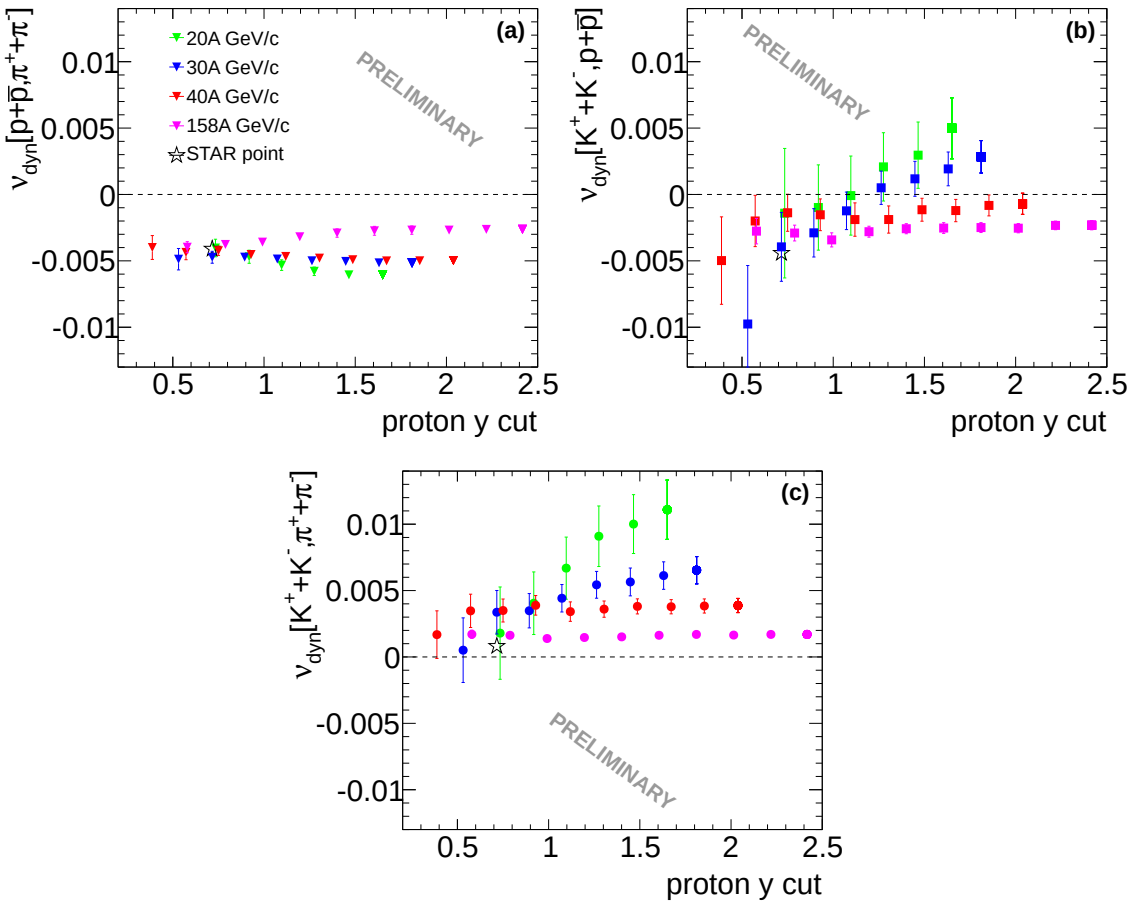

Figure 13. (Color Online) Phase-space region dependence of (a) $\nu_{dyn}[p+\bar{p},\pi^{+}+\pi^{-}]$, (b) $\nu_{dyn}[K^{+}+K^{-},p+\bar{p}]$ and (c) $\nu_{dyn}[K^{+}+K^{-},\pi^{+}+\pi^{-}]$ in central Pb+Pb collisions of NA49 (triangles, squares, dots). Stars show measurements of the STAR collaboration. Results are plotted versus the maximum proton rapidity (see text).

remarkable that $\nu_{dyn}[p+\bar{p},\pi^{+}+\pi^{-}]$ shows little dependence on the covered phase space region. This detailed study of ν_{dyn} in different phase space regions appears to explain to a large extent the difference between the STAR BES and NA49 measurements.

Some final remarks are in order concerning the properties and the significance of the fluctuation measure ν_{dyn}. To reveal the underlying physics from the study of event-by-event fluctuations, the obtained fluctuation signals from heavy-ion (A+A) collisions should be compared systematically to a reference from nucleon-nucleon (N+N) collisions at corresponding energies per nucleon. It is however important to properly take into account trivial differences between A+A and N+N collisions e.g., in the size of the colliding systems. In

thermodynamics the quantities which are proportional to the volume (size) of the system are called extensive quantities. For example, the mean number of particles in a relativistic gas within the Grand Canonical Ensemble (GCE) is an extensive quantity. The ratio of two extensive quantities does not depend on the system volume and is referred to as an intensive quantity. The studied fluctuation measure ν_{dyn} is more complicated because it is inversely proportional to the number of wounded nucleons, in a wounded nucleon model. An additional complication in the experimental study of fluctuations in A+A collisions are unavoidable volume fluctuations from event to event. These additional sources of fluctuations may well mask the fluctuation of interest. For example, the scaled variance defined in Eq.(8) is an intensive quantity, but it is sensitive to the fluctuations of volume. On the other hand, within the GCE, the value of ν_{dyn} does not depend on volume fluctuations. However, it does depend on the volume itself (see the text above). It is rather suggestive to normalize ν_{dyn} in order to remove the volume dependence but still keep it independent of volume fluctuations (within the GCE):

$$\nu_{dyn}[A,B]^{Scaled} = \frac{\nu_{dyn}[A,B]}{\frac{1}{<A>} + \frac{1}{<B>}} \tag{15}$$

Note that Eq.(15) is a reformulated variant of Eq.(14).

The fluctuation measure Σ^{AB} proposed in Ref. [21] depends neither on the system volume nor on its fluctuations (in the GCE or within the wounded nucleon model). Interestingly, using the definition of ν_{dyn} from Eq.(12) and the scaling property for ν_{dyn} (see Eq.(15)), one finds that Σ and the rescaled ν_{dyn} are practically the same fluctuation measures:

$$\nu_{dyn}[A,B]^{Scaled} = \Sigma^{AB} - 1 \tag{16}$$

IX. SUMMARY

In summary several scenarios were investigated to understand the differences between the NA49 and STAR measurements of the excitation functions of $\nu_{dyn}[p,K]$ and $\nu_{dyn}[\pi,K]$. For this purpose the particle identification procedure formerly employed by NA49 was replaced by a different approach, the Identity Method, to reconstruct the fluctuation measure ν_{dyn}. The increasing trend of $\nu_{dyn}[p,K]$ and $\nu_{dyn}[\pi,K]$ towards lower energies reported in previous publications of NA49 in terms of the quantity σ_{dyn} was confirmed by this analysis. A detailed

study of ν_{dyn} reveals a strong dependence on the phase space coverage at low energies for $\nu_{dyn}[p, K]$ and $\nu_{dyn}[\pi, K]$ which might explain the different energy dependences measured by NA49 (central Pb+Pb collisions) and STAR (BES program for central Au+Au collisions). As an outlook it is worth mentioning that since the Identity Method allows to reconstruct first and second moments of the multiplicity distributions of identified particles one will be able to investigate the energy dependence of all the fluctuation measures proposed in Ref. [21]. These quantities are better suited for phase transition studies because (within the grand canonical ensemble) they depend neither on the volume nor on its fluctuations which cannot be tightly controlled in experiments.

A. Acknowledgments

This work was supported by the US Department of Energy Grant DE-FG03-97ER41020/A000, the Bundesministerium fur Bildung und Forschung (06F 137), Germany, the German Research Foundation (grant GA 1480/2.1), the National Science Centre, Poland (grants DEC-2011/03/B/ST2/02617 and DEC-2011/03/B/ST2/02634), the Hungarian Scientific Research Foundation (Grants OTKA 68506, 71989, A08-77719 and A08-77815), the Bolyai Research Grant, the Bulgarian National Science Fund (Ph-09/05), the Croatian Ministry of Science, Education and Sport (Project 098-0982887-2878) and Stichting FOM, the Netherlands.

REFERENCES

[1] for recent results see: C. Schmidt (RBC-Bielefeld and HotQCD Collaborations), Nucl. Phys. A820, 41c (2009); Z. Fodor and S. Katz (Wuppertal Collaboration), Acta Phys. Pol. B42, 2791 (2011).

[2] M. Stephanov, Int. J. Mod. Phys. A20, 4387 (2005).

[3] M. Stephanov, K. Rajagopal and E. Shuryak, Phys. Rev. D60, 114028 (1999).

[4] V. Koch, arXiv:0810.2520 (2008).

[5] U. Heinz and M. Jacob, arXiv:nucl-th/0002042 (2000).

[6] M. Gazdzicki and M. Gorenstein, Acta Phys. Pol. B30, 2705 (1999).

[7] C. Alt et al. (NA49 Collab.), Phys. Rev. C77, 024903 (2008).

[8] A. Rustamov, Central Eur. J. Phys. 10, 1267-1270 (2012), arXiv:1201.4520v1 [nucl-ex] (2012).

[9] C. Alt et al. (NA49 Collab.), Phys. Rev. C79, 044910 (2009).

[10] T. Anticic et al. (NA49 Collab.) Phys. Rev. C83, 061902(R) (2011).

[11] T. Anticic et al. (NA49 Collab.), Phys. Rev. C87, 024902 (2013).

[12] T. J Tarnowsky (STAR Collab.) J. Phys. G: Nucl. Part. Phys. 38 124054 (2011).

[13] C. Pruneau, S. Gavin, S. Voloshin, PRC 66, 044904 (2002).

[14] M. Gazdzicki et al., Phys. Rev. C83, 054907 (2011).

[15] M. I. Gorenstein, Phys. Rev. C84, 024902 (2011).

[16] S. Afanasiev et al. (NA49 Collab.), Nucl. Instrum. Meth. A430, 210 (1999).

[17] L. Landau, Journal of Physics (USSR), vol. 8, p. 201 (1944).

[18] M. van Leeuwen, PhD thesis, NIKHEFF, Amsterdam (2003), CERN EDMS Id 816033; NA49 technical notes G. Veres, CERN EDMS Id 815871 (2000), M. van Leeuwen, CERN EDMS Id 983015.

[19] A. Rustamov, M. I. Gorenstein, Phys. Rev. C86, 044906 (2012).

[20] V. Koch and T. Schuster, Phys. Rev. C81, 034910 (2010).

[21] M. I. Gorenstein and M. Gazdzicki, Phys.Rev. C84, 014904 (2011).